research papers

Structural studies on *Mycobacterium tuberculosis* DXR in complex with the antibiotic FR-900098

Christofer Björkelid, Terese Bergfors, Torsten Unge, Sherry L. Mowbray and T. Alwyn Jones*

Department of Cell and Molecular Biology, Uppsala University, Biomedical Center, Box 596, SE-751 24 Uppsala, Sweden

Correspondence e-mail: alwyn@xray.bmc.uu.se

A number of pathogens, including the causative agents of tuberculosis and malaria, synthesize the essential isoprenoid precursor isopentenyl diphosphate *via* the 2-*C*-methyl-D-erythritol 4-phosphate (MEP) pathway rather than the classical mevalonate pathway that is found in humans. As part of a structure-based drug-discovery program against tuberculosis, DXR, the enzyme that carries out the second step in the MEP pathway, has been investigated. This enzyme is the target for the antibiotic fosmidomycin and its active acetyl derivative FR-900098. The structure of DXR from *Mycobacterium tuberculosis* in complex with FR-900098, manganese and the NADPH cofactor has been solved and refined. This is a new crystal form that diffracts to a higher resolution than any other DXR complex reported to date. Comparisons with other ternary complexes show that the conformation is that of the enzyme in an active state: the active-site flap is well defined and the cofactor-binding domain has a conformation that brings the NADPH into the active site in a manner suitable for catalysis. The substrate-binding site is highly conserved in a number of pathogens that use this pathway, so any new inhibitor that is designed for the *M. tuberculosis* enzyme is likely to exhibit broad-spectrum activity.

1. Introduction

Two pathways exist for the synthesis of isopentenyl diphosphate (IPP), an activated isoprene unit that is a key building block for the essential isoprenoids. A now-classical pathway was first described that proceeds *via* the intermediate mevalonate (Beytía & Porter, 1976), but a different route was later identified that is used in Gram-negative and some Gram-positive bacteria, as well as in plant chloroplasts, algae and apicomplexan protozoa (Rohmer, 1999). This second pathway is used by a number of pathogens to convert pyruvate and glyceraldehyde 3-phosphate into IPP in seven steps, each catalysed by an enzyme that is not present in humans. The possibility of developing new drugs that specifically target the enzymes in this pathway was supported by the discovery that the antibiotic fosmidomycin inhibits the second (and the first committed) step in the pathway (Kuzuyama *et al.*, 1998; Zeidler *et al.*, 1998), in which 1-deoxy-D-xylulose 5-phosphate (DXP) is converted to 2-*C*-methyl-D-erythritol 4-phosphate (MEP) by the enzyme 1-deoxy-D-xylulose-5-phosphate reducto-isomerase (DXR, also called IspC; Fig. 1*a*). Since then, this so-called non-mevalonate or MEP pathway has been extensively studied in the hope of producing new drugs and herbicides.

The efficient DXR inhibitor FR-900098 was isolated from a *Streptomyces* strain during a screening program designed to

identify new antibiotics that interfere with bacterial cell-wall synthesis (Okuhara *et al.*, 1980*a*). This success prompted further screening of *Streptomyces* strains from other soil samples, which produced three related compounds with antibacterial activity (Kuroda *et al.*, 1980; Okuhara *et al.*, 1980*b*), of which FR-31564 was the most active. FR-31564 {renamed fosmidomycin; 3-[formyl(hydroxy)amino]propylphosphonic acid; FOM} and its acetyl derivative FR-900098 {*i.e.* 3-[acetyl-(hydroxy)amino]propylphosphonic acid; F98} are simple compounds containing a phosphonate group connected to a retro-hydroxamic acid group *via* a three-methylene linker (Kamiya *et al.*, 1980; Iguchi *et al.*, 1980) that closely mimic in size and character the substrate and reaction product of DXR (Fig. 1). Both show antibacterial activity against most Gram-negative and some Gram-positive bacteria (Okuhara *et al.*, 1980*b*) and can inhibit the growth of *Plasmodium* species *in vitro* and *in vivo* (Jomaa *et al.*, 1999). Clinical trials in combination with clindamycin show that fosmidomycin has efficacy and is tolerated for the treatment of *P. falciparum* malaria (Borrmann *et al.*, 2004), but cannot be used as a single drug treatment because of rapid clearance from the parasite and recrudescent infection (Lell *et al.*, 2003). Unfortunately, these antibiotics are not active against all bacteria that rely solely on the MEP pathway. In particular, they have no activity against *Mycobacterium tuberculosis*, the causative agent of tuberculosis (TB), which is estimated to kill two million people every year. Despite this lack of biological activity, which has been attributed to poor uptake (Brown & Parish, 2008), both antibiotics are good inhibitors of *M. tuberculosis* DXR (*Mt*DXR; Dhiman *et al.*, 2005; Henriksson *et al.*, 2006, 2007; Andaloussi *et al.*, 2011). Indeed, the well conserved active site of DXR leads us to believe that a medicinal chemistry effort aimed at finding better inhibitors for *Mt*DXR may produce compounds with interesting effects on other pathogens in which the MEP pathway is essential. As part of this Same-Target-Other-Pathogen (STOP) strategy, we have reported the structure determination of the *Mt*DXR apoenzyme (Henriksson *et al.*, 2006) and a second crystal form that included fosmidomycin in a ternary complex with NADPH (Henriksson *et al.*, 2007), followed by structures with two fosmidomycin analogues (one of which was solved in two different crystal forms; Andaloussi *et al.*, 2011). A structure including one of these analogues was also solved using our expression construct and crystallization conditions by Deng, Diao *et al.* (2011). These studies, and extensive studies on the *Escherichia coli* enzyme, show that DXR is subject to conformational changes owing to both movements in an active-site flap and rigid-body motions of functional domains. To expand our understanding of DXR specificity and to provide new insights into the conformational variation within DXRs in general and *Mt*DXR in particular, we have searched for new crystallization conditions and new ligand complexes that are suitable for crystallographic studies. Here, we report the structure determination of *Mt*DXR in complex with the antibiotic FR-900098, NADPH and manganese in a new crystal form, which diffracts to the highest resolution achieved to date for any structure of this enzyme from any species.

2. Methods

2.1. Crystallization

The *Mt*DXR protein was expressed and purified as described previously (Henriksson *et al.*, 2007). The construct encoded an N-terminal His$_6$ tag followed by residues 1–389 of the *Rv2870c* gene sequence originating from *M. tuberculosis* strain H37R (*i.e.* 24 amino acids were deleted from the C-terminus). After the final purification step, the protein was concentrated to 0.12–0.14 m*M* in 10 m*M* Tris–HCl pH 7.4, 100 m*M* NaCl, 2–10% glycerol and 1 m*M* MnCl$_2$.

Vapour-diffusion crystallization trials were set up in sitting drops at 293 K. The reservoirs of the two-well MRC plates (Molecular Dimensions, UK) were filled manually with 80 µl reservoir solution, after which the crystallization droplets were dispensed using an Oryx 6 robot (Douglas Instruments, UK) and the plate was sealed. The droplet volume was 0.65 µl; it was composed of 0.3 µl each of the protein and reservoir solutions and 0.05 µl seed stock [made from apo-DXR microcrystals grown in 25%(*w*/*v*) PEG 3350, 200 m*M* sodium or potassium acetate, 100 m*M* bis-tris pH 5.7, 1% tacsimate]. The antibiotic FR-900098 was dissolved in 100% dimethyl sulfoxide (DMSO) to a final concentration of 100 m*M*. To obtain crystals of *Mt*DXR in complex with active-site manganese ion, FR-900098 and NADPH (*Mt*DXR–Mn–F98–NADPH), the NADPH cofactor (1 m*M*) and FR-900098 (2.5 m*M* final concentration in 2.5% DMSO) were added to the protein solution before screening. Crystals (0.1 × 0.1 × 0.1 mm in size) grew in 1–2 d from various conditions in the Morpheus screen (Molecular Dimensions, UK; Gorrec, 2009), the best of which was E1 [10%(*w*/*v*) PEG 20 000, 20%(*v*/*v*) monomethyl ether PEG 550, 0.1 *M* MES–imidazole pH 6.5 and 0.03 *M* each of diethylene glycol, triethylene glycol, tetraethylene glycol and pentaethylene glycol]. The reservoir solution (Morpheus E1) also served as the cryoprotectant.

2.2. Crystallographic analysis

Diffraction data for the *Mt*DXR–Mn–F98–NADPH complex were collected from a single crystal at the European Synchrotron Radiation Facility (ESRF). The diffraction images were indexed and integrated using *MOSFLM* (Leslie,
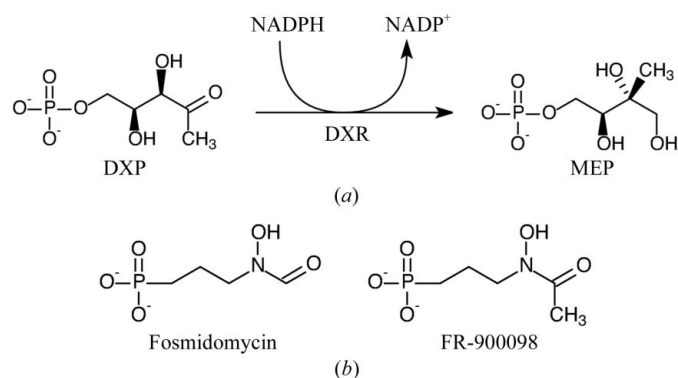
Figure 1
(*a*) The second step in the MEP pathway, catalysed by DXR. (*b*) Structures of fosmidomycin and FR-900098.

2006) and scaled with *SCALA* (Evans, 2006), which are both part of the *CCP*4 package (Winn *et al.*, 2011). The complex crystallized as a new form in space group $P4_32_12$ with a complete dimer in the asymmetric unit. The structure was solved by molecular replacement using *Phaser* (McCoy *et al.*, 2007) using the *A* chain of the earlier *Mt*DXR–Mn–FOM–NADPH ternary-complex structure (PDB entry 2jcz, stripped of waters and ligands; Henriksson *et al.*, 2007) as the search model. The resulting model was improved by alternating restrained reciprocal-space refinement with *REFMAC*5 (Murshudov *et al.*, 2011) and manual rebuilding with *O* (Jones *et al.*, 1991). Stereochemical restraints for the antibiotic were generated in *O* with the *QDS* tools and the fitted model was then used to generate restraints for refinement using a suitably edited dictionary generated by *REFMAC*5. The hydroxamic group was restrained to planarity with target standard deviations of 0.02 Å. Metal-coordination target distances were taken from Harding (2006) and used with standard deviations of 0.02 Å. Waters were added using the profile-based methods developed by Jones and implemented in *O*. Because of the high resolution of this study, noncrystallographic restraints were not used during the refinement. Six residues were refined with dual conformations (Arg14 in the *A* chain, Arg341 in the *B* chain and Thr26 and Leu174 in both chains), none of which are in the active site. Two close contacts were observed in the final model. One involves a water molecule (*B*2125, with a temperature factor of 21.5 Å) positioned 2.02 Å from the NE2 atom of His191 in the *B* chain, which may indicate a modification of the imidazole ring. The second involves a pair of water molecules (*A*2151 and *A*2244, with temperature factors of 28.2 and 32.8 Å, respectively) separated by 1.90 Å that are located in a small sausage-shaped density and may indicate partial occupancies.

Detailed structural comparisons were made using the *LSQ* commands in *O* with default C^α matching-pair cutoffs of 3.8 Å or with a close-pair cutoff of 1.0 Å (Kleywegt & Jones, 1997). Sequence alignment was performed with *ClustalW* (Larkin *et al.*, 2007) and the corresponding figure was made with *ALINE* (Bond & Schüttelkopf, 2009). Other figures were created in *O* and rendered with *Molray* (Harris & Jones, 2001). Secondary-structure assignments were made with the *yasspa* command in *O* and are drawn with red–blue rainbow colouring for one chain. Data-collection and refinement statistics for the complex are given in Table 1.

3. Results

3.1. *Mt*DXR–Mn–F98–NADPH complex

We have previously reported three crystal forms of *Mt*DXR. The first was obtained using the full-length enzyme, with which we were unable to obtain interesting ligand complexes. Instead, a sulfate ion from the crystallization medium was located at the binding site for the phosphate group of the natural substrate (Henriksson *et al.*, 2006). A shorter construct was later crystallized in two additional forms, both of which allowed structure determination of inhibitor

Table 1
Data-collection and refinement statistics for *Mt*DXR–Mn–F98–NADPH (PDB entry 4a03).

Values in parentheses are for the outer resolution shell.

Data-collection statistics	
Beamline	ID23-1, ESRF
Detector	ADSC Q315r
Wavelength (Å)	0.9768
Space group	$P4_32_12$
Unit-cell parameters (Å)	$a = b = 110.5$, $c = 137.0$
V_M† (Å^3 Da^{-1})	2.44
Resolution range (Å)	42.2–1.65 (1.74–1.65)
No. of reflections measured	795061
No. of unique reflections	101922
Average multiplicity	7.8 (7.9)
Completeness (%)	99.8 (100.0)
R_{merge}‡§	0.087 (0.461)
R_{meas}¶	0.094 (0.494)
$R_{p.i.m.}$††	0.034 (0.176)
$\langle I/\sigma(I)\rangle$	14.4 (4.6)
Refinement statistics	
Resolution range (Å)	42.2–1.65 (1.69–1.65)
No. of reflections used in working set	96739 (7109)
No. of reflections for R_{free} calculation	5087 (332)
R (%)	18.9
R_{free} (%)	21.6
No. of non-H atoms	6263
No. of solvent waters	529
Mean B factors (Å^2)	
Protein atoms (*A*, *B*)	18.5, 24.4
Solvent atoms	29.9
FR900098 (*A*, *B*)	15.3, 18.0
NADPH (*A*, *B*)	15.6, 23.5
Glycerol (*A*, *B*)	34.9, —
Ramachandran plot outliers‡‡ (*A*, *B*) (%)	0.6, 0.6
R.m.s.d. from ideal bond length§§ (Å)	0.007
R.m.s.d. from ideal bond angle (°)	1.16

† Matthews (1968). ‡ Merging and crystallographic R factors were generated using the computer programs described in §2. § $R_{merge} = \sum_{hkl} \sum_i |I_i(hkl) - \langle I(hkl)\rangle| / \sum_{hkl} \sum_i I_i(hkl)$. ¶ $R_{meas} = \sum_{hkl} \{N/[N(hkl) - 1]\}^{1/2} \sum_i |I_i(hkl) - \langle I(hkl)\rangle| / \sum_{hkl} \sum_i I_i(hkl)$. †† $R_{p.i.m.} = \sum_{hkl} \{1/[N(hkl) - 1]\}^{1/2} \sum_i |I_i(hkl) - \langle I(hkl)\rangle| / \sum_{hkl} \sum_i I_i(hkl)$. ‡‡ Calculated using a strict-boundary Ramachandran plot definition (Kleywegt & Jones, 1996). §§ Ideal values from Engh & Huber (1991).

complexes even though one of them included ammonium sulfate in the crystallization medium (Henriksson *et al.*, 2007; Andaloussi *et al.*, 2011). In both new crystal forms the asymmetric unit contained a dimer in which one active site is in a closed conformation and the other is in an open conformation; only the more closed molecule showed the presence of bound inhibitors. The structural framework for our medicinal chemistry efforts has therefore been based on a structure with a well defined active-site flap, as exemplified by molecule *A* of the *Mt*DXR–Mn–FOM–NADPH ternary complex (Henriksson *et al.*, 2007), and complexes with two fosmidomycin analogues in different crystal forms in which the flap is disordered (Andaloussi *et al.*, 2011). These analogues correspond to formyl and acetyl variants of the dichlorophenyl α-aryl-substituted fosmidomycin derivatives described by Haemers *et al.* (2006). We chose to study the natural product antibiotic FR-900098, the acetyl derivative of fosmidomycin that differs only by the addition of a methyl group near the hydroxamic acid (Kamiya *et al.*, 1980; Fig. 1*b*), to determine whether these equivalent small changes would also be associated with a disordered loop. At the same time, we carried out a new crystallization search in an attempt to produce alternative

conditions that would be useful for future studies of inhibitor complexes.

The *Mt*DXR–Mn–F98–NADPH complex represents such a new crystal form. These conditions have produced the best diffracting DXR crystals published to date and we are therefore able to describe the complex structure at unusually high resolution for this enzyme (Table 1). The structure was solved by molecular replacement and refined to R and R_{free} values of 18.9% and 21.6%, respectively, at 1.65 Å resolution. As with all of our other crystal forms, the crystal contains a complete dimer in the asymmetric unit. However, both active sites are in closed conformations, rather than the usual closed and open views associated with the previous crystals that contained inhibitors. We therefore obtain two views of the active site, each in complex with FR-900098 and NADPH. The separate chains, corresponding to residues 11–388, can be superimposed with a root-mean square deviation (r.m.s.d.) of 0.37 Å on C^α atoms *via* an almost perfect twofold rotation (179.7°). Density is lacking for ten residues at each N-terminus and one residue at each C-terminus. The fit of the model to the electron density is very good (Fig. 2), except for the edge helix of the NADPH-binding domain in the *B* subunit (residues *B*74– *B*80). The active-site flap, which is often disordered in the available DXR structures (Reuter *et al.*, 2002), is well ordered in both chains. The three domains of individual DXR chains often slide as rigid bodies relative to one another in the different crystal forms, which we describe with the aid of a yardstick measurement across the NADPH-binding site (between the C^α atoms of residues 47 and 339 in *Mt*DXR, equivalent to residues 36 and 348 in *Ec*DXR; Henriksson *et al.*, 2007). This distance is 20.0 and 19.8 Å for the two molecules of our new complex, compared with values in the range 20.3–25.0 Å for our earlier structures. These are therefore the most closed conformations that we have observed for the *Mt*DXR enzyme. Presumably because of different crystal contacts, the *B* subunit has slightly higher average temperature factors than the *A* chain (Table 1).

The active sites are essentially identical in the two subunits, with the main interactions between the enzyme and antibiotic shown in Fig. 3(*a*). The metal-ion coordination is the same as that described previously for both fosmidomycin and dichlorophenyl analogues, with manganese-to-oxygen distances in the range 1.95–2.20 Å. The binding of the hydroxamic acid group of the antibiotic restricts access, which means that for steric reasons only five O atoms coordinate each metal ion, with an approximate octahedral geometry. While the protein ligands show geometric deviations from ideal values that are in the range 6–15°, the coordination geometry around the hydroxamic acid group is more distorted. The N-hydroxyl O atom of FR-900098 is positioned opposite Glu153, with the coordinating O atoms subtending angles of 142° with the manganese ion and

117° with the carboxyl O atom of Asp151. The *N*-formyl O atom is opposite Glu222 and shows less distortion, subtending angles of 84, 99 and 160° with the coordinating carboxyl O atoms of Asp151, Glu153 and Glu222, respectively. The hydroxamic acid group adopts a synperiplanar conformation, with an O=C—N—O torsion angle of 0°. The *N*-formyl O atom accepts a hydrogen bond from the Ser152 hydroxyl, while the phosphonate group forms a network of nine hydrogen bonds with protein and solvent, including salt links to the His200 and Lys219 side chains (Fig. 3*a*). Each O atom of the phosphonate group is involved in two hydrogen bonds to protein atoms and one to a solvent molecule. The interaction network is therefore very similar to that described for fosmidomycin binding to *Mt*DXR (Henriksson *et al.*, 2007). Even the solvent structure in the active site is highly conserved, including the water molecules in the so-called conserved water pocket, as well as those in the substrate- and cofactor-binding sites. The entire active-site flap (residues 199–208) is very well defined in the electron density. In particular, the indole ring of Trp203 shields the antibiotic from the external solvent, while the imidazole ring of His200 interacts with the phosphonate. The methyl group of the hydroxamic acid points towards the indole ring, making close contacts of 3.2 and 3.3 Å with the CE2 and CD2 atoms, respectively (Figs. 2 and 3*a*). The complete NADPH is also very well defined (density for just the nicotinamide ring of the cofactor associated with the *A* chain is shown in Fig. 2, but is indicative of the quality for the rest of the molecule) and maintains essentially all of the protein and water interactions that were observed in the fosmidomycin ternary complex. The improved resolution allows us to identify four new waters that form hydrogen bonds to the cofactor and three interactions that are present in both complexes but are close to the hydrogen-bond distance cutoff used in the preparation of the relevant figure in Henriksson *et al.* (2007). The differences in the active sites of the FR-900098 and fosmidomycin complexes are minor: small changes in the side
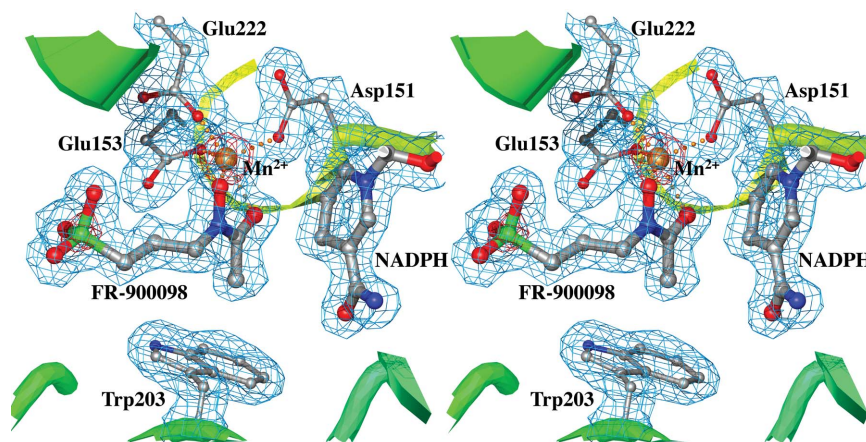
Figure 2
Representative electron density in the *Mt*DXR–Mn–F98–NADPH structure. The σ_A-weighted $(2m|F_o| - D|F_c|)$ electron-density map (Read, 1986) is drawn at levels of 0.35 e Å^{-3} (the root-mean-square value of the map, in light blue) and 2.50 e Å^{-3} (in red) around the FR-900098 binding site. The background cartoon has been created with a red–blue rainbow colouring for one chain. The secondary-structural elements have been defined as described in §2 and as drawn in Fig. 5.

chain of Asp151 at the metal ion and small rearrangements of the next shell of side chains that interact with the metal-ion-coordinating residues. In particular, there are small changes in the interacting Asp151–Glu225–Lys128 cluster. A re-evaluation of the density for the *Mt*DXR–Mn–FOM–NADPH ternary complex suggests that these differences are not all real. The side chain of Lys128 can be remodelled in the fosmidomycin-complex structure to fit its density in a conformation more similar to that in the FR-900098 complex. In this conformation the NZ atom of the lysine forms salt links with the carboxylates of two of the residues that coordinate the metal ion: Asp151 and Glu222.

3.2. Relationship to earlier structures

The two molecules in the *Mt*DXR–Mn–F98–NADPH structure are very similar to the closed subunit of the *Mt*DXR–Mn–FOM–NADPH ternary complex. Their respective *A* chains, corresponding to residues 11–388, can be super-

imposed with an r.m.s.d. of 0.39 Å on C$^{\alpha}$ atoms. Both antibiotics bind to *Mt*DXR in the DXP-binding site, making essentially the same specific interactions with the enzyme at the phosphonate and hydroxamic acid groups. The carbon backbones of the inhibitors have very similar conformations, with each being shielded from the external solvent as described above. Only the change from the formyl group of fosmidomycin to the acetyl group of FR-900098 introduces new interactions with the enzyme (Fig. 3*a*), which are localized to the indole ring of Trp203.

Our *Mt*DXR ternary complexes are most similar to the closed *Ec*DXR–DXP–NADPH and *Ec*DXR–FOM–NADPH ternary complexes described by Mac Sweeney *et al.* (2005), which lack an active-site metal ion, and the recent *Pf*DXR–Mg–F98–NADPH and *Pf*DXR–Mg–FOM–NADPH ternary complexes described by Umeda *et al.* (2011). The active site and NADPH-binding domains have the same relative orientations and the active-site flaps have essentially identical structures (Fig. 4*a*). For example, the *A* chain of *Mt*DXR–Mn–F98–NADPH (residues *A*11–*A*388) matches well with the complexes of *Ec*DXR (*Ec*DXR–DXP–NADPH; PDB entry 1q0q; r.m.s.d. of 1.45 Å over 356 C$^{\alpha}$ atoms; Mac Sweeney *et al.*, 2005) and *Pf*DXR (*Pf*DXR–Mg–F98–NADPH; PDB entry 3aua; r.m.s.d. of 1.37 Å over 352 C$^{\alpha}$ atoms; Umeda *et al.*, 2011). The new high-resolution structures thus allow us to more confidently describe the water structure in the active sites, as well as the specific ligand–enzyme interactions, most of which are conserved (Fig. 3). The lack of a metal ion in the *Ec*DXR ternary complexes does not allow us to view the coordination in these cases, but the coordinations of the antibiotics at the active-site metal of the *Pf*DXR ternary complexes are the same as those first described in the *Mt*DXR–Mn–FOM–NADPH ternary complex of Henriksson *et al.* (2007), as well as those in the *Mt*DXR–Mn–F98–NADPH structure described above. The respective phosphonate–enzyme interactions are very similar in all of these complexes, although there are some subtle differences. In the metal-free *Ec*DXR–DXP–NADPH complex, for example, the phosphate group forms the same nine hydrogen-bond/salt-link interactions as observed in the *Mt*DXR ternary complexes [although the equivalent main-chain amide hydrogen bond from Ser177 (*M. tuberculosis* numbering) is slightly longer (3.2 Å) in the *Ec*DXR complex]. After superimposing the C$^{\alpha}$ atoms of the enzymes, the P atoms are then only 0.10 Å apart and the interacting groups are closely superimposable (Fig. 4*a*). However, in the *Pf*DXR ternary complexes only two
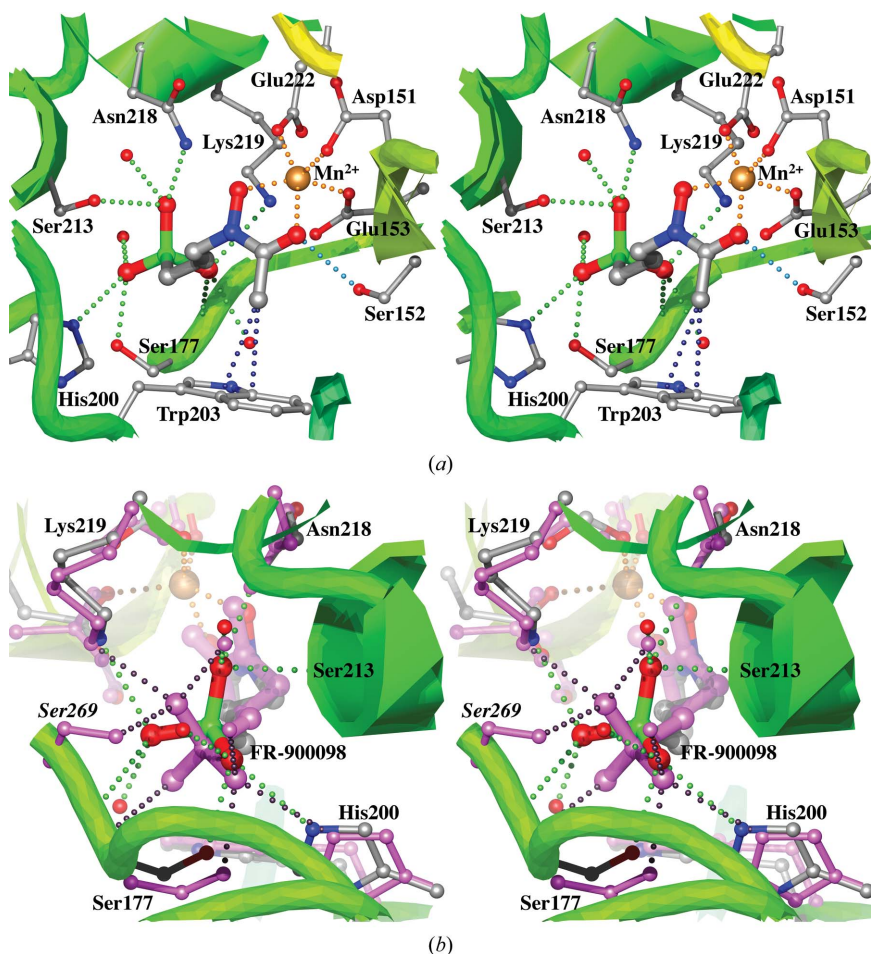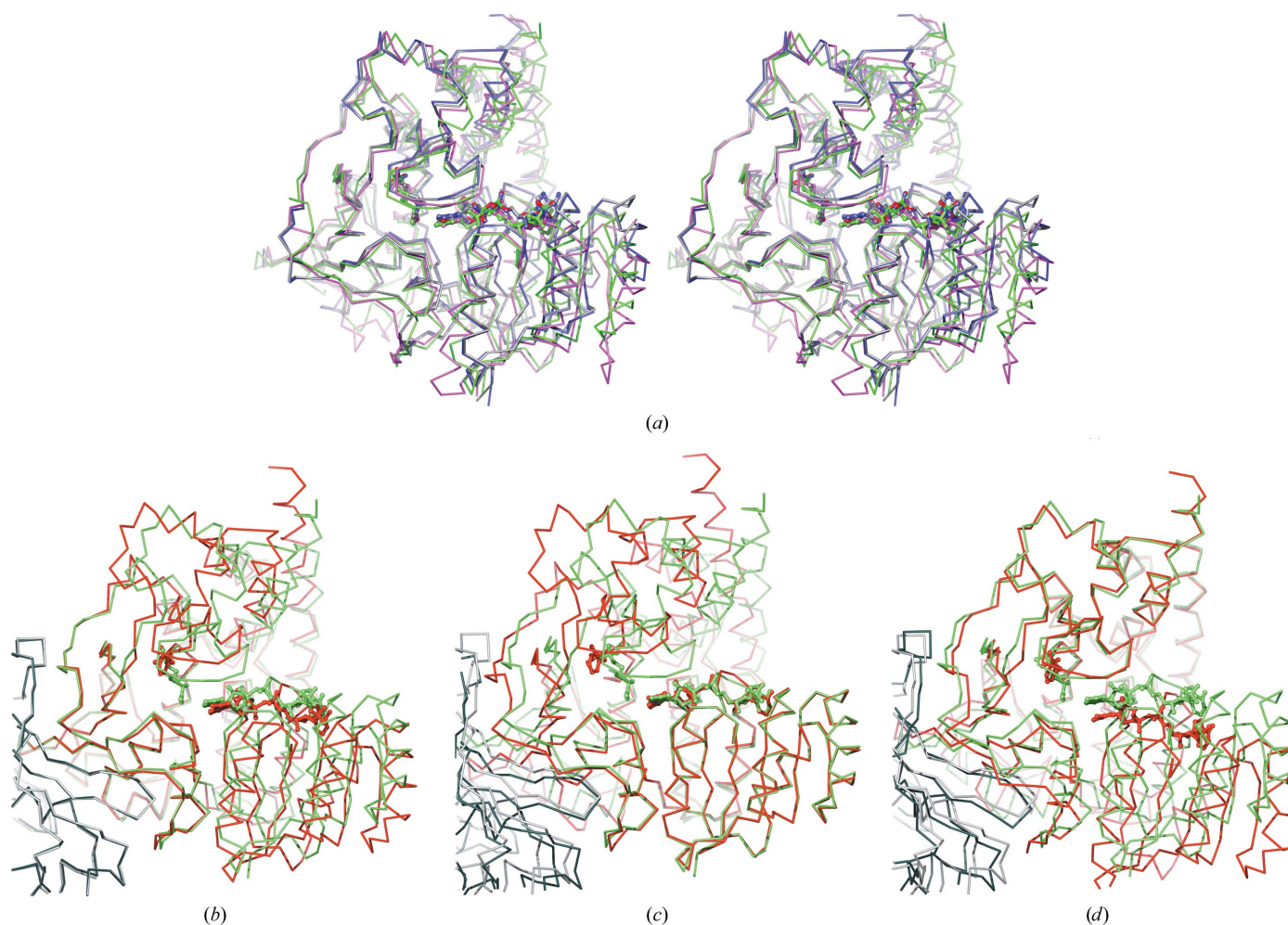

Figure 3
(*a*) Interactions of FR-900098 with *Mt*DXR, showing side chains and waters that interact with the antibiotic. Hydrogen bonds or salt links with the phosphonate are shown as lime green bubbled lines, while those involving the metal are coral-coloured. The interactions of the acetylhydroxyamino group are indicated in navy blue for the closest van der Waals contacts with the indole ring of Trp203 and in sky blue for the hydrogen bond to the hydroxyl group of Ser152. (*b*) Overlay of the *Mt*DXR–Mn–F98–NADPH (PDB entry 4a03, atom colouring) and *Pf*DXR–Mg–F98–NADPH (PDB entry 3aua, violet colouring) structures, showing residues that interact with the FR-900098 phosphonate group.

phosphonate O atoms have the full complement of hydrogen-bonding donors, in each case two from the enzyme and one from a water molecule (Fig. 3*b*). The third O atom has only one hydrogen bond from the enzyme (the main-chain amide of *Pf*DXR Ser270, equivalent to Ser177 in *Mt*DXR), as well as a single water from the FOM complex (the equivalent water is 3.35 Å from the phospho oxygen in the FR-900098 complex). Interestingly, only one phosphonate O atom has identical partners in the *Mt*DXR and *Ec*DXR enzymes, involving Ser177 and His200 in *Mt*DXR (residues 270 and 293 in *Pf*DXR; Fig. 3*b*). These changes arise as a consequence of the Ala→Ser mutation at Ala176 in *Mt*DXR (Ser269 in *Pf*DXR; Fig. 5). A new hydrogen-bonding group is thereby introduced at the phosphonate-binding site of *Pf*DXR, which results in a new set of interactions (Fig. 3*b*). The phosphonate O atom that accepts the hydrogen bond from the hydroxyl of this serine also interacts with the highly conserved lysine residue

corresponding to Lys219 in *Mt*DXR, as well as a structurally conserved water molecule (although this solvent interacts with a different phosphonate O atom in *Pf*DXR compared with *Mt*DXR and *Ec*DXR). The mutation and resulting adaption means that the highly conserved side chains corresponding to Ser213 and Asn218 in *Mt*DXR do not contribute to phosphonate-group hydrogen bonding in *Pf*DXR.

3.3. Structure-based alignment of DXR sequences

In Fig. 5, we have aligned DXR sequences from a selected number of pathogens to help us evaluate if our observations are relevant within a STOP strategy for drug discovery. Fig. 3 shows the key residues within the enclosed substrate-binding site that interact with the antibiotics, which we have classified into four groups. Group 1 residues directly coordinate the active-site metal (Asp151, Glu153 and Glu222 in *Mt*DXR
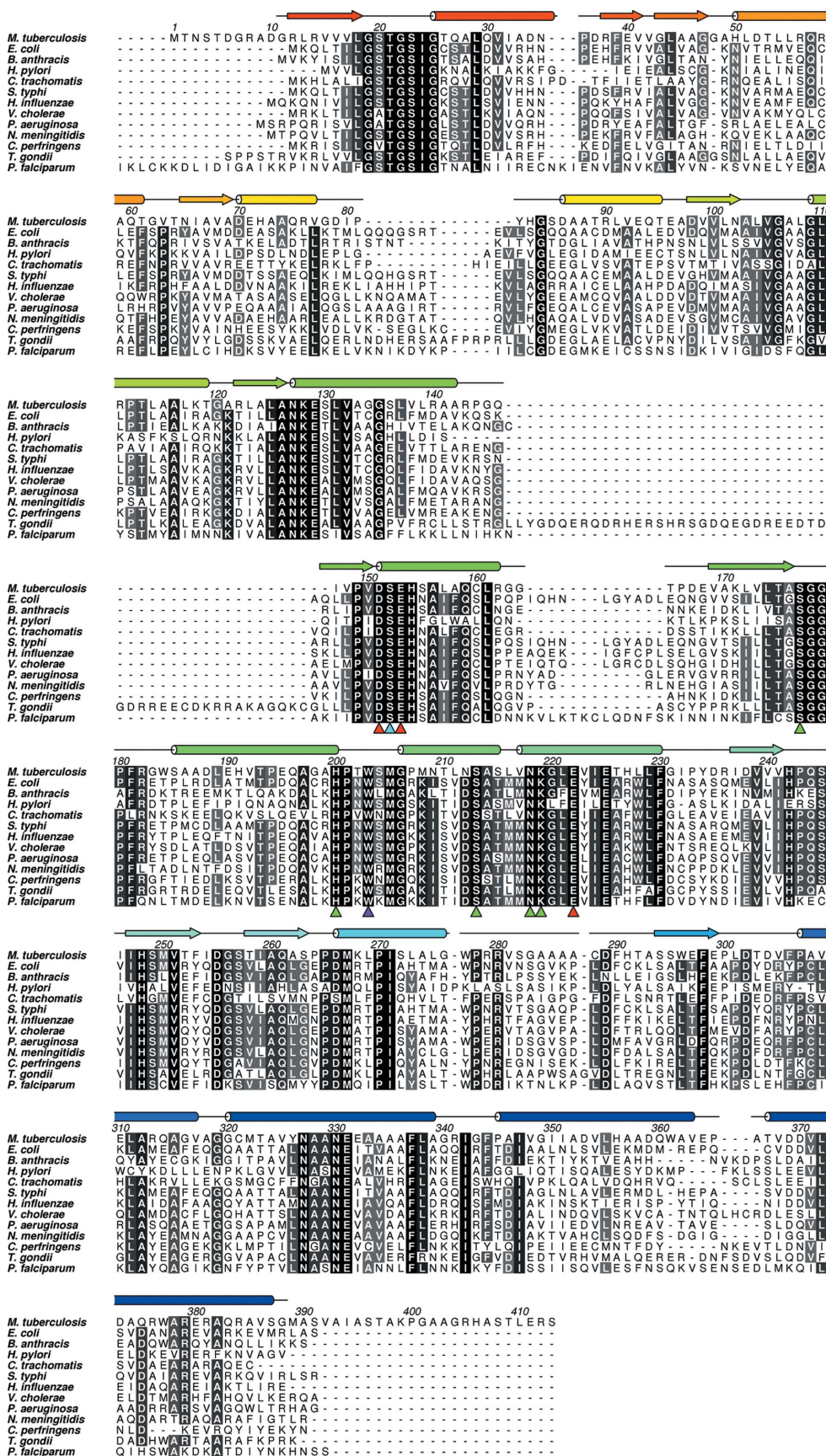

(a)

(b)

(c)

(d)

Figure 4
(*a*) C$^\alpha$ superposition of the *Mt*DXR–Mn–F98–NADPH (PDB entry 4a03; grey), *Mt*DXR–Mn–FOM–NADPH (PDB entry 2jcz; blue), *Ec*DXR–DXP–NADPH (PDB entry 1q0q; green) and *Pf*DXR–Mg–F98–NADPH (PDB entry 3aua; violet) structures. The superpositions were made with the close-pair cutoff described in §2. (*b*) C$^\alpha$ superposition of whole dimers of *Ec*DXR–DXP–NADPH (PDB entry 1q0q; green) and *Ec*DXR-(pyridin-2-yl-methylphosphonic acid)-NADPH (PDB entry 3anl; red) complexes. Cofactors and ligands are shown. The superposition was made with the close-pair cutoff described in §2. (*c*) C$^\alpha$ superposition of single NADPH-binding domains of the *Ec*DXR–DXP–NADPH (PDB entry 1q0q; green) and *Ec*DXR–(pyridin-2-yl-methylphosphonic acid)–NADPH (PDB entry 3anl; red) complexes. Cofactors and ligands are shown. (*d*) C$^\alpha$ superposition of single C-terminal domains of EcDXR–DXP–NADPH (PDB entry 1q0q; green) and EcDXR–(pyridin-2-yl-methylphosphonic acid)–NADPH (PDB entry 3anl; red) complexes. Cofactors and ligands are shown.

numbering) and are all conserved in the sequences. Group 2 residues interact with the antibiotic, either with the phosphonate group (Ser177, His200, Ser213, Asn218 and Lys219) or with other parts of the drug (Ser152 and Trp203), and are also fully conserved. A third group, however, are slightly more distant from the antibiotic, but with side chains pointing inwards (Ala176, Gly179, Met205, Asn209 and Met267). These are also fully conserved, except for Ala176 and Asn209. The equivalent residue to Ala176 in *Pf*DXR is a serine, which donates a hydrogen bond to the phosphonate group of FOM/F98 as discussed above; all other species have an alanine or glycine at this position. Residue Asn209 in *Mt*DXR is clearly an outlier in terms of sequence conservation; however, the more usual isoleucine residue is easily accommodated in the cavity, where it helps to define the binding site for the nicotinamide ring of the NADPH cofactor. The final group have side chains that line the conserved water pocket (Henriksson *et al.*, 2007); of these residues (Thr175, Ser245 and

Figure 5
Alignment of DXR sequences from selected pathogens. The numbering scheme and secondary-structural elements are from *Mt*DXR. Secondary-structural elements are coloured as in Figs. 2 and 3. Red triangles show residues involved in coordination of the Mn^{2+} ion. Green triangles show residues interacting with the phosphonate group of FR-900098. The blue triangle shows Ser152 interacting with the hydroxamic acid part of FR-900098. The violet triangle shows Trp203 in the active-site flap. *Mycobacterium tuberculosis*, *Mt*DXR (UniProt ID P64012); *Escherichia coli*, *Ec*DXR (UniProt ID P45568); *Bacillus anthracis*, *Ba*DXR (UniProt ID Q81N10); *Helicobacter pylori*, *Hp*DXR DXR (UniProt ID P56139); *Chlamydia trachomatis*, *Ct*DXR (UniProt ID O84074); *Salmonella typhi*, *St*DXR (UniProt ID Q8Z9A6); *Haemophilus influenzae*, *Hi*DXR (UniProt ID Q4QM93); *Vibrio cholerae*, *Vc*DXR (UniProt ID Q9KPV8); *Pseudomonas aeruginosa*, *Pa*DXR (UniProt ID Q9KGU6); *Neisseria meningitidis*, *Nm*DXR (UniProt ID Q9JX33); *Clostridium perfringens*, *Cp*DXR (UniProt ID Q8XJR1); *Toxoplasma gondii*, *Tg*DXR (UniProt ID B6KSI3); *Plasmodium falciparum*, *Pf*DXR (UniProt ID O96693).

His248), the first two show slight variation. Other fully conserved residues in Fig. 5 include those making up the second-layer interactions around the metal ligands (Lys128, His154 and Glu225) and those that interact with the cofactor (Glu129 and others). In particular, in the ternary complexes the nicotinamide ring of the cofactor slots into a cavity lined with the side chains of Met205 and Asn209 'above' the ring and Ile24 and Met267 'below' the ring, all of which are highly conserved. Elsewhere in the alignments, we can identify structural reasons for conservation (cis-proline at Pro278 and glycine preferences, for example), as well as interactions that are specific for the family as a whole. For example, Asp255 is fully conserved while Arg280 shows just a single variation, a consequence of the fact that these side chains interact across the dimer interface to form a fully buried salt link. Similarly, Phe298 is located on a strand on the dimer interface that is involved in hydrophobic side-chain interactions with residues 290 and 296 from the other subunit (the latter are all hydrophobic in the alignments).

4. Discussion

DXR is a challenging target for structure-based drug discovery, in part because of its conformational flexibility. The enzyme is a homodimer in which each subunit is built up from three domains. The N-terminal portion of the sequence comprises an NADPH-binding domain and the C-terminal regions form a small helical domain, while the central core represents a dimer-forming domain. If we use the domain definitions of Steinbacher et al. (2003), this central domain also contains the residues of the active site. Comparison of the published structures of DXR shows that these domains are loosely coupled, sliding with respect to each other by essentially rigid-body motions (Henriksson et al., 2007; Takenoya et al., 2010). A simple yardstick, the distance between selected points in the N- and C-terminal domains (the C^α atoms of residues 47 and 339, respectively, in MtDXR), can be used to measure the degree of opening of the NADPH-binding site (Henriksson et al., 2007). The most studied, EcDXR, shows a large variation, ranging from an ultra-open apoenzyme conformation (Reuter et al., 2002) to the much more closed structure of a ternary complex lacking the active-site metal ion (Mac Sweeney et al., 2005). Further dynamics are evident in a short loop that acts as a flap over the substrate-binding site. In many crystal forms the residues making up this loop, some of which are highly conserved between species, are not observed in the electron density or have elevated temperature factors. The NADPH, on the other hand, 'rides' on its binding site located on the edge of the N-terminal domain, so that as a result of rigid-body movement of the domain as a whole the cofactor can swing closer to the substrate (Fig. 4), as described in more detail below. It is not unusual to observe that in the same crystal, active sites show different degrees of opening. In two of the crystal forms that we have previously described for MtDXR we observed a complete dimer in the crystallographic asymmetric unit in which the active sites differed; only the more closed subunit binds inhibitors (Henriksson et al., 2007;

Andaloussi et al., 2011). In contrast, in the FR-900098 complex described here we observe a dimer of the ternary complex in which both active sites are in the closed state and the active-site flaps are both very well defined. The new crystal form will therefore be particularly useful for future structural studies of MtDXR in complex with new fosmidomycin analogues.

The change from the formyl group of fosmidomycin to the acetyl group of FR-900098 has the potential to interfere with the indole ring of Trp203, a highly conserved residue in the active-site flap of all DXRs (Fig. 5), and even to destabilize the active-site flap. However, in our activity assay FR-900098 has only a twofold higher IC_{50} towards MtDXR than fosmidomycin (160 and 80 nM, respectively; Andaloussi et al., 2011), and the structure shows clearly that the flap is not destabilized. The close contacts of the newly introduced methyl group with the indole ring of Trp203 (Figs. 2 and 3) are within the hard-sphere van der Waals contact distance, which could account for the slight decrease in affinity. The recently published structure of the PfDXR–Mg–F98–NADPH complex (Umeda et al., 2011) shows an interaction between the equivalent indole ring and the antibiotic that is essentially identical to that we see here. However, this interaction is also remarkably similar to that seen for DXP (which also has a methyl group in this position; Fig. 1) in the EcDXR–DXP–NADPH ternary complex (Mac Sweeney et al., 2005; Fig. 4a). Here, the lack of a metal ion gives greater freedom to optimize the energetics of the interaction of the substrate with the enzyme, so the high degree of similarity in the complexes suggests that the methyl–indole interaction may in fact be close to optimal. In published studies on EcDXR, FR-900098 has inhibitory activity similar to (Haemers et al., 2008) or better than (Behrendt et al., 2010) fosmidomycin. It is well known that FR-900098 is highly active in the P. falciparum in vitro growth-inhibition assay as well as in in vivo efficacy studies (Verbrugghen et al., 2010). Behrendt et al. (2010) reported IC_{50} values of 15 nM for FR-900098 compared with 144 nM for fosmidomycin towards the PfDXR enzyme, so the observed contacts with the methyl group are clearly not detrimental to activity in this case either. These authors also describe swapped hydroxamic acid analogues; an acetyl derivative in this series has the best enzyme inhibition and in vitro growth IC_{50} values reported to date: 3 and 590 nM, respectively. These low values cannot be a result of favourable interactions with the conserved tryptophan ring, however, since this C^α phenyl-ring analogue is likely to destabilize the flap (Andaloussi et al., 2011; Behrendt et al., 2011).

The seven independent views that we now have for DXR ternary complexes [two metal-free EcDXR DXS and FOM complex structures (Mac Sweeney et al., 2005), two of MtDXR in FOM and F98 complexes containing manganese and one in an FOM complex lacking the active-site ion, and two of PfDXR in FOM and F98 complexes containing magnesium] reinforce the view that the model described by Henriksson et al. (2007) more closely describes the mode of binding of the substrate than does the model of Steinbacher et al. (2003) based on the lower resolution EcDXR–FOM binary complex. In the latter the flap is not as well defined and not as closed, so the complete set of interactions with the inhibitor that are

shown in Fig. 3(a) are not formed. The relative orientation of the active-site and NADPH-binding domains is also different in this binary complex, such that a bound cofactor would not be positioned to act as a hydride donor in the enzymatic reaction. The introduction of the cofactor into a complex, however, is not sufficient to force the enzyme into a functional conformation. In a series of *Ec*DXR phosphonate-compound complexes with NADPH, Deng, Endo *et al.* (2011) observed structures that lack metal ions and have the NADPH-binding domain swung further away from the active site. The aromatic rings of these bound phosphonates form face-to-face inter-actions with the indole ring of Trp211 (*Ec*DXR numbering) in a flap that is not in a functional conformation (Fig. 4b). The phosphonate group of these inhibitors, however, is localized to the phosphate/phosphonate-binding site of the substrate and fosmidomycin analogues that we, as well as Mac Sweeney and coworkers, have described in detail (Fig. 3a). In the conformations trapped by Deng, Endo *et al.* (2011), NADPH is further from the substrate as a result of a rigid-body rotation of the whole NADPH-binding domain by ∼8° around an axis that passes close to the active site (PDB entry 3anl; Figs. 4b and 4c). The NADPH 'rides' on its binding site located on the edge of this N-terminal domain, so that the cofactor swings closer to the substrate. As a consequence, the distance between the C4N nicotinamide hydride donor and the N1 atom of the antibiotic, which approximates the position of the acceptor in the reaction mechanism, decreases from approximately 5.1 to 3.7 Å. Similarly, the C-terminal helical domain is displaced by an ∼9° rotation that dislodges the flap from the conformation needed for activity (Figs. 4b and 4d). Except for the active-site flap, the relative orientations of the domains observed by Deng, Endo *et al.* (2011) are very similar to those observed in the binary complex of Steinbacher *et al.* (2003), so that 359 C^α atoms of each respective *A* chain can be super-imposed with an r.m.s.d. of 0.44 Å. Interestingly, in both these studies the structures were produced by soaking crystals with the inhibitor of interest.

The *Mt*DXR and *Pf*DXR ternary complexes described above show that the acetyl derivative of fosmidomycin (*i.e.* FR-900098) can be accommodated in the active site of these enzymes without disrupting the flap. Larger groups would be expected to clash with Trp203, which is borne out by the loss of *Ec*DXR inhibition in fosmidomycin derivatives with larger, more lipophilic acyl-group extensions (Ortmann *et al.*, 2007). Similarly, modifying the number of linking C atoms between the phosphonate and hydroxamic acid groups lowers activity, with a reduction in the number of methylene units being more detrimental than an increase by one unit (Zinglé *et al.*, 2010; Bodill *et al.*, 2011). This is a consequence of the fact that the carbon backbones of FR-900098 and fosmidomycin are almost fully extended (Fig. 3a) and are fixed at both ends by inter-actions with their phosphonate and hydroxamic acid groups. Except for the new methyl group, the detailed interactions made by the antibiotics with *Mt*DXR (Fig. 3a) are essentially identical both at the hydroxamic acid group as well as at their respective phosphonate groups. Verbrugghen *et al.* (2010) have estimated the pK_{a2} of FR-900098 to be 7.35 using the pH-

dependence of the ^{31}P chemical shift. However, in the highly polar positively charged environment of the DXR binding site the pK_{a2} is expected to be lower and the group is likely to carry a double negative charge under physiological conditions. The conserved interactions observed for *Ec*DXR–DXP–NADPH and *Mt*DXR ternary complexes in crystals produced at pH 6.5 and 5.7–6.5, respectively, suggest the same double negatively charged state. However, in the *Ec*DXR–FOM–NADPH complex, which was crystallized at pH 5.0, the metal ion was absent (although magnesium was present in the crystallization drop) and there are slight changes in the coordination around the phosphonate group. In particular, the equivalent interaction with His209 in *Ec*DXR (equivalent to His200 in *Mt*DXR) is missing and there is a rearrangement of the side-chain conformation of Ser222 in *Ec*DXR (equivalent to Ser213 in *Mt*DXR). These changes were interpreted as a consequence of the lower pH of this study compared with that of the substrate ternary complex, which resulted in a mono-anionic phosphonate species (Mac Sweeney *et al.*, 2005). The magnesium-ion-containing *Pf*DXR ternary complexes were solved with crystals obtained at a pH of ∼8.0, where the phosphonate groups of FR-900098 and fosmidomycin would be doubly charged. The doubly charged phosphonate group is indeed a key factor in achieving high activity for fosmido-mycin analogues. Designs that replace it with an uncharged or single negatively charged group result in a sharp drop in activity (Perruchon *et al.*, 2008; Zinglé *et al.*, 2010). The much-reduced activity of sulfonate analogues, for example, does not require a discussion of subtle variations in hydrogen-bonding distances and interactions. Rather, it follows directly from the charged state of the analogue and the environment in which it must bind. The close concentration of hydrogen-bond donors and salt-link interactions that are observed in the ternary complexes explains the preference for a double negatively charged phosphonate group at this position. Electron-with-drawing substitutions that have been designed to decrease the pK_a of the phosphonate group do give rise to improved anti-malarial activity (Haemers *et al.*, 2006; Verbrugghen *et al.*, 2010). The introduction of a large α-aryl substitution such as a 3,4-dichlorophenyl group, however, forces large structural changes in the active site of the enzyme (Andaloussi *et al.*, 2011; Deng, Diao *et al.*, 2011) which are likely to be more relevant than a slight charge modulation. Even small changes, such as in the α-halogenated analogues of FR-900098 described by Verbrugghen *et al.* (2010), may result in altera-tions in the binding site that are more significant than an effect owing to charge modulation.

Finally, the new crystal form that we have described in this publication, together with the structure-based sequence alignments presented in Fig. 5, strengthens our belief that *Mt*DXR provides a good basis for a STOP drug-discovery program that aims to exploit inhibitor binding at the substrate-binding site of this essential enzyme.

References

Andaloussi, M., Henriksson, L. M., Więckowska, A., Lindh, M., Björkelid, C., Larsson, A. M., Suresh, S., Iyer, H., Srinivasa, B. R., Bergfors, T., Unge, T., Mowbray, S. L., Larhed, M., Jones, T. A. & Karlén, A. (2011). *J. Med. Chem.* **54**, 4964–4976.

Behrendt, C. T., Kunfermann, A., Illarionova, V., Matheeussen, A., Gräwert, T., Groll, M., Rohdich, F., Bacher, A., Eisenreich, W., Fischer, M., Maes, L. & Kurz, T. (2010). *ChemMedChem*, **5**, 1673–1676.

Behrendt, C. T., Kunfermann, A., Illarionova, V., Matheeussen, A., Pein, M. K., Gräwert, T., Kaiser, J., Bacher, A., Eisenreich, W., Illarionov, B., Fischer, M., Maes, L., Groll, M. & Kurz, T. (2011). *J. Med. Chem.* **54**, 6796–6802.

Beytía, E. D. & Porter, J. W. (1976). *Annu. Rev. Biochem.* **45**, 113–142.

Bodill, T., Conibear, A. C., Blatch, G. L., Lobb, K. A. & Kaye, P. T. (2011). *Bioorg. Med. Chem.* **19**, 1321–1327.

Bond, C. S. & Schüttelkopf, A. W. (2009). *Acta Cryst.* D**65**, 510–512.

Borrmann, S., Issifou, S., Esser, G., Adegnika, A. A., Ramharter, M., Matsiegui, P. B., Oyakhirome, S., Mawili-Mboumba, D. P., Missinou, M. A., Kun, J. F., Jomaa, H. & Kremsner, P. G. (2004). *J. Infect. Dis.* **190**, 1534–1540.

Brown, A. C. & Parish, T. (2008). *BMC Microbiol.* **8**, 78.

Deng, L., Diao, J., Chen, P., Pujari, V., Yao, Y., Cheng, G., Crick, D. C., Prasad, B. V. & Song, Y. (2011). *J. Med. Chem.* **54**, 4721–4734.

Deng, L., Endo, K., Kato, M., Cheng, G., Yajima, S. & Song, Y. (2011). *ACS Med. Chem. Lett.* **2**, 165–170.

Dhiman, R. K., Schaeffer, M. L., Bailey, A. M., Testa, C. A., Scherman, H. & Crick, D. C. (2005). *J. Bacteriol.* **187**, 8395–8402.

Engh, R. A. & Huber, R. (1991). *Acta Cryst.* A**47**, 392–400.

Evans, P. (2006). *Acta Cryst.* D**62**, 72–82.

Gorrec, F. (2009). *J. Appl. Cryst.* **42**, 1035–1042.

Haemers, T., Wiesner, J., Giessmann, D., Verbrugghen, T., Hillaert, U., Ortmann, R., Jomaa, H., Link, A., Schlitzer, M. & Van Calenbergh, S. (2008). *Bioorg. Med. Chem.* **16**, 3361–3371.

Haemers, T., Wiesner, J., Van Poecke, S., Goeman, J., Henschker, D., Beck, E., Jomaa, H. & Van Calenbergh, S. (2006). *Bioorg. Med. Chem. Lett.* **16**, 1888–1891.

Harding, M. M. (2006). *Acta Cryst.* D**62**, 678–682.

Harris, M. & Jones, T. A. (2001). *Acta Cryst.* D**57**, 1201–1203.

Henriksson, L. M., Björkelid, C., Mowbray, S. L. & Unge, T. (2006). *Acta Cryst.* D**62**, 807–813.

Henriksson, L. M., Unge, T., Carlsson, J., Aqvist, J., Mowbray, S. L. & Jones, T. A. (2007). *J. Biol. Chem.* **282**, 19905–19916.

Iguchi, E., Okuhara, M., Kohsaka, M., Aoki, H. & Imanaka, H. (1980). *J. Antibiot.* **33**, 19–23.

Jomaa, H., Wiesner, J., Sanderbrand, S., Altincicek, B., Weidemeyer, C., Hintz, M., Türbachova, I., Eberl, M., Zeidler, J., Lichtenthaler, H. K., Soldati, D. & Beck, E. (1999). *Science*, **285**, 1573–1576.

Jones, T. A., Zou, J.-Y., Cowan, S. W. & Kjeldgaard, M. (1991). *Acta Cryst.* A**47**, 110–119.

Kamiya, T., Hemmi, K., Takeno, H. & Hashimoto, M. (1980). *Tetrahedron Lett.* **21**, 95–98.

Kleywegt, G. J. & Jones, T. A. (1996). *Structure*, **4**, 1395–1400.

Kleywegt, G. J. & Jones, T. A. (1997). *Methods Enzymol.* **277**, 525–545.

Kuroda, Y., Okuhara, M., Goto, T., Okamoto, M., Terano, H., Kohsaka, M., Aoki, H. & Imanaka, H. (1980). *J. Antibiot.* **33**, 29–35.

Kuzuyama, T., Shimizu, T., Takahashi, S. & Seto, H. (1998). *Tetrahedron Lett.* **39**, 7913–7916.

Larkin, M. A., Blackshields, G., Brown, N. P., Chenna, R., McGettigan, P. A., McWilliam, H., Valentin, F., Wallace, I. M., Wilm, A., Lopez, R., Thompson, J. D., Gibson, T. J. & Higgins, D. G. (2007). *Bioinformatics*, **23**, 2947–2948.

Lell, B., Ruangweerayut, R., Wiesner, J., Missinou, M. A., Schindler, A., Baranek, T., Hintz, M., Hutchinson, D., Jomaa, H. & Kremsner, P. G. (2003). *Antimicrob. Agents Chemother.* **47**, 735–738.

Leslie, A. G. W. (2006). *Acta Cryst.* D**62**, 48–57.

Mac Sweeney, A., Lange, R., Fernandes, R. P., Schulz, H., Dale, G. E., Douangamath, A., Proteau, P. J. & Oefner, C. (2005). *J. Mol. Biol.* **345**, 115–127.

Matthews, B. W. (1968). *J. Mol. Biol.* **33**, 491–497.

McCoy, A. J., Grosse-Kunstleve, R. W., Adams, P. D., Winn, M. D., Storoni, L. C. & Read, R. J. (2007). *J. Appl. Cryst.* **40**, 658–674.

Murshudov, G. N., Skubák, P., Lebedev, A. A., Pannu, N. S., Steiner, R. A., Nicholls, R. A., Winn, M. D., Long, F. & Vagin, A. A. (2011). *Acta Cryst.* D**67**, 355–367.

Okuhara, M., Kuroda, Y., Goto, T., Okamoto, M., Terano, H., Kohsaka, M., Aoki, H. & Imanaka, H. (1980a). *J. Antibiot. (Tokyo)*, **33**, 13–17.

Okuhara, M., Kuroda, Y., Goto, T., Okamoto, M., Terano, H., Kohsaka, M., Aoki, H. & Imanaka, H. (1980b). *J. Antibiot. (Tokyo)*, **33**, 24–28.

Ortmann, R., Wiesner, J., Silber, K., Klebe, G., Jomaa, H. & Schlitzer, M. (2007). *Arch. Pharm. (Weinheim)*, **340**, 483–490.

Perruchon, J., Ortmann, R., Altenkämper, M., Silber, K., Wiesner, J., Jomaa, H., Klebe, G. & Schlitzer, M. (2008). *ChemMedChem*, **3**, 1232–1241.

Read, R. J. (1986). *Acta Cryst.* A**42**, 140–149.

Reuter, K., Sanderbrand, S., Jomaa, H., Wiesner, J., Steinbrecher, I., Beck, E., Hintz, M., Klebe, G. & Stubbs, M. T. (2002). *J. Biol. Chem.* **277**, 5378–5384.

Rohmer, M. (1999). *Nat. Prod. Rep.* **16**, 565–574.

Steinbacher, S., Kaiser, J., Eisenreich, W., Huber, R., Bacher, A. & Rohdich, F. (2003). *J. Biol. Chem.* **278**, 18401–18407.

Takenoya, M., Ohtaki, A., Noguchi, K., Endo, K., Sasaki, Y., Ohsawa, K., Yajima, S. & Yohda, M. (2010). *J. Struct. Biol.* **170**, 532–539.

Umeda, T., Tanaka, N., Kusakabe, Y., Nakanishi, M., Kitade, Y. & Nakamura, K. T. (2011). *Sci. Rep.* **1**, 9.

Verbrugghen, T., Cos, P., Maes, L. & Van Calenbergh, S. (2010). *J. Med. Chem.* **53**, 5342–5346.

Winn, M. D. *et al.* (2011). *Acta Cryst.* D**67**, 235–242.

Zeidler, J., Schwender, J., Muller, C., Wiesner, J., Weidemeyer, C., Beck, E., Jomaa, H. & Lichtenthaler, H. K. (1998). *Z. Naturforsch. C*, **53**, 980–986.

Zinglé, C., Kuntz, L., Tritsch, D., Grosdemange-Billiard, C. & Rohmer, M. (2010). *J. Org. Chem.* **75**, 3203–3207.